Editors' Suggestion

Quantum Monte Carlo Study of Positron Lifetimes in Solids

K. A. Simula,* J. E. Muff, and I. Makkonen
Department of Physics, University of Helsinki, P.O. Box 43, Helsinki FI-00014, Finland

N. D. Drummond
Department of Physics, Lancaster University, Lancaster LA1 4YB, United Kingdom

(Received 12 July 2021; revised 27 May 2022; accepted 22 September 2022; published 14 October 2022)

We present an analysis of positron lifetimes in solids with unprecedented depth. Instead of modeling correlation effects with density functionals, we study positron-electron wave functions with long-range correlations included. This gives new insight in understanding positron annihilation in metals, insulators, and semiconductors. By using a new quantum Monte Carlo approach for computation of positron lifetimes, an improved accuracy compared to previous computations is obtained for a representative set of materials when compared with experiment. Thus, we present a method without free parameters as a useful alternative to the already existing methods for modeling positrons in solids.

DOI: 10.1103/PhysRevLett.129.166403

Positron annihilation is an elementary component of quantum electrodynamics [1]. Measurable annihilation parameters such as positron annihilation rate and momentum density of annihilation radiation are governed by many-body interactions between the positron and the surrounding electronic system. Theoretical predictions and experimental measurements can provide a good match for few-electron systems; for example, the binding energies of positrons bound to molecules can be reproduced [2]. Theoretical studies of homogeneous electron-positron systems provide a starting point for understanding positron annihilation in more complex systems [3,4], but real, inhomogeneous systems are nevertheless often problematic. Better description of the correlations is needed to improve theory and applicability of positron physics.

Positron annihilation spectroscopy [5] is a powerful, nondestructive method for studying systems including metals, alloys, semiconductors and insulators [6], polymers and soft matter [7,8], and porous materials [9]. The method involves injecting positrons into a sample where they first thermalize rapidly and then either continue diffusing as a delocalized wave or become trapped in voidlike open volumes. Eventually, each positron annihilates with an electron, emitting two detectable 511 keV γ photons. As the positrons are very sensitive to open volumes within a sample, measured lifetime components and their intensities provide information on the size and concentration of vacancies trapping the positrons [5].

Positron lifetime techniques can be combined with, for example, *in situ* irradiation [10] or optical illumination [11] to study damage production and various defect properties. Pulsed slow positron beams [12] can be used for lifetime studies of thin films or scanning surfaces with a micrometer-scale lateral resolution [13]. Also the study of pore size distribution in thin films is possible [9]. On the other hand, the local electronic momentum density of the annihilation site is directly connected to the Doppler broadening of the annihilation γ radiation, enabling the study of the chemical surroundings of lattice defects [5] or Fermi surfaces of metals [14].

Theoretical models associate measured lifetime components to microscopic traps in the material. Single-particle models, such as Hartree-Fock (HF) theory, ignore many-body correlation effects between particles. Such models give smaller positron-electron overlaps, overestimating the positron lifetimes by nearly an order of magnitude [15]. Better description of positrons is provided by two-component density functional theory (DFT) [3], where the many-body correlation effects are included in approximate correlation functionals of the particle densities. In the local density approximation (LDA), the electron-positron correlation energies are obtained from functionals of the local densities, and the electron-positron overlap enhanced by correlations is computed with another local functional, the so-called enhancement factor. Generalized gradient approximations (GGAs) [16–18] can improve lifetime calculations in comparison to the underlying LDA parametrizations.

Despite successes with LDA or GGA functionals, DFT is an insufficient theory for positron annihilation studies. A correlation functional may accurately predict the lifetime in some systems while failing in others. The lifetimes by different functionals in a given system can differ even by 30 ps (see below). Moreover, there is no *a priori* means to determine a functional best suited for a given task, but experimental benchmarking is needed; and the construction of a functional can require both higher level calculations, such as quantum Monte Carlo calculations [4], and fits to experimental data [18].

For a given positron lifetime setup, the statistical accuracy achievable for a defect-free sample is on the order of 1 ps. In general, DFT does not reach this accuracy. Moreover, local or semilocal correlation functionals are bound to fail in solid-state systems with large open volumes or surfaces. Thus, often it is not possible to adequately assign the components of the measured lifetime spectra to different microstructures of the sample. Development of a practical many-body theory that is accurate and able to describe complex correlation effects has been a long-standing problem in the field of positron physics and its applications. More accurate many-body theory could improve the applicability of positron annihilation and provide new research areas. For example, the correlation functionals could be evaluated and improved using a more descriptive theory. A many-body theory also enables the study of positrons in systems with multideterminantal nature, impossible with current methods but unavoidable with many lattice defects [19].

Importantly, the dependence of positron lifetime on lattice vibrations is a theoretical question unaddressed to date and should clearly be studied for complete understanding of positron annihilation in solids.

We present quantum Monte Carlo (QMC) as a new method, devoid of free parameters, for simulation of positrons in solids. To our knowledge, this is the first QMC study of positrons in real crystals, although such studies exist for molecules [20,21] and electron gases [4]. Calculation of positron lifetimes in the perfect bulk of materials is the first and the most critical test for benchmarking how well the electron-positron correlations in inhomogeneous solid-state systems can be described before we move on to other experimentally relevant quantities, such as the momentum density of annihilating pairs. Annihilation studies in defect systems, such as vacancies, in which also the detailed ionic structure in the presence of the trapped positron poses a challenge, can follow after we have validated the capability of QMC to describe correlations in defect-free lattices.

We perform a detailed study of finite-size effects involved and how to best describe annihilation with core electrons. Besides QMC, we study vibrational effects on positron lifetime.

The studies were performed for C and Si in the diamond structure, body-centered cubic Li, and wurtzite AlN, a set that consists of materials of past and present interest in the field of positron annihilation spectroscopy and includes insulators (C), semiconductors (AlN, Si), and metals (Li). The choice of the test set was limited by the need of experimental reference data and by the available pseudopotentials. Si and AlN have well-known experimental reference results. C is a less correlated system and expected to be easy to model with QMC. The positron lifetime in Li has been overestimated by many state of-the-art two-component DFT correlation functionals, making the results by QMC theoretically interesting.

We use variational and diffusion Monte Carlo (VMC and DMC) methods [22,23] as implemented in the CASINO code [24,25]. The fermion-sign problem is treated in DMC by imposing a fixed-node approximation [26] that constrains the nodal surface of the wave function to be that of the VMC-optimized wave function.

The VMC many-body wave functions are represented as Slater-Jastrow (SJ) or Slater-Jastrow-backflow (SJB) wave functions [27,28]. The former is a product of single-particle Slater determinants and a Jastrow factor. The determinants fix the nodal surface, and the Jastrow factor is a parametrized function describing the interparticle correlations. The SJB wave function goes beyond the single-particle SJ nodal surface by introducing parametrized shifts into the particle coordinates. Optimizing backflow parameters both increases variational freedom in VMC and reduces the DMC fixed-node error.

The trial wave functions can be written for a system with one positron as

$$\begin{aligned}\Psi_{\mathrm{SJ}}(\mathbf{R}) &= e^{J(\mathbf{R})}[\phi^l(\mathbf{r}_{i\uparrow})][\phi^m(\mathbf{r}_{j\downarrow})]\phi(\mathbf{r}_+),\\ \Psi_{\mathrm{SJB}}(\mathbf{R}) &= e^{J(\mathbf{R})}[\phi^l(\mathbf{r}_{i\uparrow}-\boldsymbol{\xi}_{i\uparrow}(\mathbf{R}))][\phi^m(\mathbf{r}_{j\downarrow}-\boldsymbol{\xi}_{j\downarrow}(\mathbf{R}))]\\ &\quad\times\phi(\mathbf{r}_+-\boldsymbol{\xi}_+(\mathbf{R})),\end{aligned}\tag{1}$$

where $\mathbf{r}_\uparrow$, $\mathbf{r}_\downarrow$, and $\mathbf{r}_+$ denote the positions of up- and down-spin electrons and the positron, respectively. N is the number of particles in the system. $\mathbf{R}$ is a $3N$-dimensional vector of the particle coordinates. $J(\mathbf{R})$ and $\boldsymbol{\xi}(\mathbf{R})$ are the Jastrow exponent and backflow displacement, respectively, parametrized with respect to different spin groupings. The ϕ functions are single-particle Kohn-Sham orbitals [29], computed with DFT using Quantum ESPRESSO [30] and our own positron package [31]. We assume that the delocalized positron density does not affect the average electron density and take the zero-positron-density limit of the $e-p$ correlation energy functional [32]. The $[\ldots]$ signs denote Slater determinants over the orbitals. The Perdew-Burke-Ernzerhof [33] GGA and Boroński-Nieminen [3] LDA functionals were used to solve electron and positron orbitals, respectively. The orbitals were in a localized B spline, or blip, basis [34] (see Supplemental Material [35]).

Periodic boundary conditions generalize the definition of orbitals in Eq. (1). Each orbital of band j at wave vector $\mathbf{k}$ $\phi^j_{\mathbf{k}}(\mathbf{r})$ is of the form $u^j_{\mathbf{k}}(\mathbf{r})e^{i\mathbf{k}\cdot\mathbf{r}}$, i.e., a lattice periodic function u multiplied by a plane wave exponential, according to Bloch's theorem. We use twist averaging, i.e., average results computed in a grid of Bloch $\mathbf{k}$ vectors, but the positron orbital is always chosen from the minimum of the parabolic positron band ($\mathbf{k}=0$), as we focus on a single thermalized positron in an infinite lattice.

The Jastrow factor contains terms representing one-, two-, and three-body correlations [38], and the backflow function contains one- and two-body terms. The Jastrow factor is optimized with a variance minimization method

(except when core electrons are included we use energy minimization, see below) [39] and the backflow is optimized together with the Jastrow factor with an energy minimization algorithm [40].

Multiple finite-size effects bias our simulations. The long-range correlations are not described correctly by finite cell sizes, and quasirandom finite-size noise arising from the forcing of Friedel oscillations to be commensurate with the simulation cell is difficult to remove from the calculation [25]. Momentum integrals are treated as discrete sums, increasing the kinetic energy bias [41]. Noise due to discrete momentum grid is reduced by twist averaging [42]. The relaxation energies are computed by fitting computed energies to the twist vectors [25] (see Supplemental Material [35]). Finite-size effects due to long-range interactions can be reduced by increasing the simulation cell size. Coulombic interactions are treated as Ewald sums, with a constant negative background charge to compensate the positive total charge due to the positron.

There are also systematic finite-size errors in energy arising from the positron interacting with its periodic images. In metallic systems, these errors should be small when the simulation cell is large compared to the Thomas-Fermi screening length. In semiconductors, the error decreases with increasing simulation cell size as $v_M/2\epsilon$, where v_M is the Madelung constant of the simulation cell that falls off with increasing number of atoms as $1/N^{1/3}$ for a given cell shape, and ϵ is the dielectric constant [25].

Norm-conserving, nonlocal Dirac-Fock average relativistic effective pseudopotentials (AREPs) [43,44] are mainly used to approximate the ion cores. The positron-nucleus interactions are calculated with inverted electron pseudopotentials. We also computed lifetimes in Si with SJ wave functions, using effective core potential (ECP) [45] pseudopotentials with two electrons within the frozen core, and performed an all-electron SJ calculation for Li, enforcing cusp conditions on the electron and positron orbitals by adding short-ranged functions [46].

The electron-positron annihilation results from the overlap of electrons and the positron in the many-body wave function [47]. The annihilation rate for 2γ annihilation is (second form given in units of ns^{-1})

$$\Gamma = \pi r_0^2 c \sum_{i=1}^{N_e} \frac{\langle \Psi | \hat{O}_i^s \delta(\mathbf{r}_i - \mathbf{r}_+) | \Psi \rangle}{\langle \Psi | \Psi \rangle} = 100.9\ g(0) \frac{N_e^{\uparrow}}{V}, \quad (2)$$

where r_0 is the classical electron radius, c is the speed of light *in vacuo*, N_e ($N_e^{\uparrow}$) is the number of individual (spin up) electrons, V is the volume of the simulation cell, and $\hat{O}_i^s$ is the spin-projection operator to the singlet state of the positron-electron pair. $g(0)$ is the rotationally and translationally averaged contact pair correlation function (PCF). In the case of metals (here Li), we make an asymptotic correction [48] and multiply the PCF with $N_e/(N_e - 1)$ to ensure that the effective electronic density is unchanged far from the positron in the simulation cell.

The system-averaged PCF $g(|\mathbf{r}_e - \mathbf{r}_p|)$ is sampled with QMC by binning electron-positron distances. The leading-order errors in Ψ_{VMC} are removed by extrapolating the final result as $g(r) = 2g_{\mathrm{DMC}}(r) - g_{\mathrm{VMC}}(r)$ [49]. The estimate of $g(|\mathbf{r}_e - \mathbf{r}_p|)$ has poor statistics near the contact region $|\mathbf{r}_e - \mathbf{r}_p| \approx 0$. We estimate the $g(0)$ by fitting an Nth-order polynomial $p(r) = a_0 - r + a_2 r^2 + \cdots + a_N r^N$ to $\log[g(r)]$ in the range $0 < r < r_{\mathrm{cut}}$, so that $g(0) = \exp(a_0)$. By setting $a_1 = -1$ in the polynomial, we assure that the fitted $\exp[p(r)]$ satisfies the Kimball cusp conditions [50]. The Supplemental Material [35] describes the details of the fitting procedure.

With pseudopotentials, the annihilation and screening interactions due to core electrons are not considered. We calculate reference DFT results and estimate the annihilation rate Γ_c due to core electrons using a number of enhancement functionals: Drummond *et al.* LDA (D-LDA) [4], Boroński-Nieminen LDA (BN-LDA) [3], Kuriplach-GGA (KUR-GGA) [17], and GGAs by Barbiellini *et al.* from Ref. [16] (B95-GGA) and [18] (B15-GGA). Hence, the total annihilation rate is $\Gamma = \Gamma_{\mathrm{QMC}} + \Gamma_c$.

For C and Si, we used $2 \times 2 \times 2$ and $3 \times 3 \times 3$ face-centered cubic (fcc) simulation cells, including 16 and 54 atoms (64 and 216 electrons with AREPs). For Si, also a $4 \times 4 \times 4$ fcc cell with 128 atoms (512 electrons) was investigated. Cubic Li $3 \times 3 \times 3$ or $5 \times 5 \times 5$ cells had 54 or 250 atoms, with one valence electron per atom. AlN was modeled with $2 \times 2 \times 1$ and $3 \times 3 \times 2$ hexagonal primitive cells, resulting in 16- and 72-atom (64- and 288-electron) supercells. ECP pseudopotential and all-electron calculations had 3 times more electrons per atom than in AREP simulations.

We have also studied the convergence of the positron relaxation energy, defined as the energy difference between a system with and without the positron, $E_r = E_+ - E_-$.

Figure 1 shows the QMC results of relaxation energies $g(0)$ and lifetimes as a function of electron number. The Monte Carlo errors are shown in the error bars. Lifetimes from DFT and experiment are also included. Twist averaging was done in a Γ-centered $4 \times 4 \times 4$ grid in the irreducible wedge of the Brillouin zone of the supercells. The backflow function was optimized separately for each twist, but with SJ wave functions the Jastrow factor optimized in the Γ point was used for all of the twists. B15-GGA was used to approximate Γ_c. Other functionals gave mainly similar results (see Supplemental Material [35]). ECP pseudopotential and all-electron results are shown against AREP results with the same number of atoms.

In AlN, Si, and Li the backflow decreases the relaxation energy by 100–400 meV and increases it by 200 meV in C. The larger cell size increases the relaxation energy by approximately 600 (C), 400 (AlN), 25 (Si), and 150 (Li)

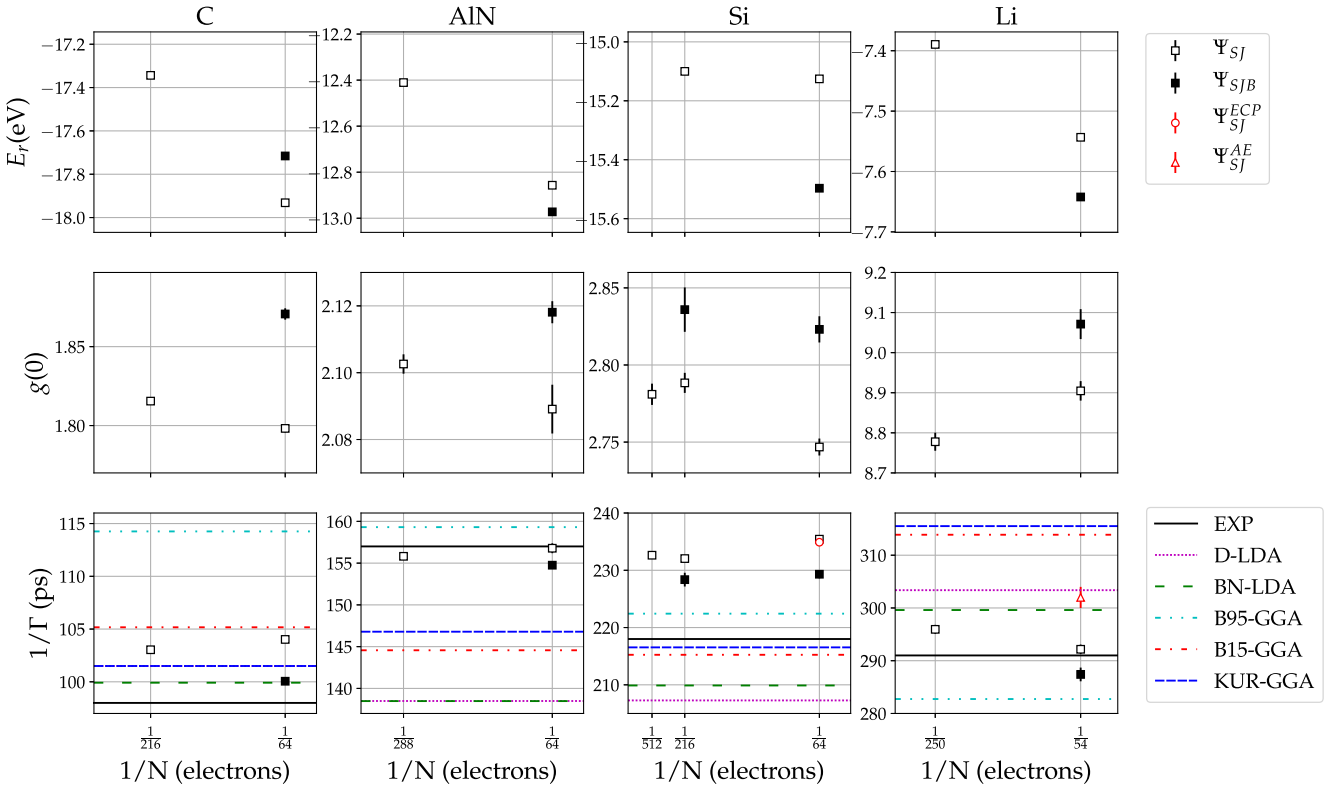

FIG. 1. Positron relaxation energies (top row), contact pair correlation functions (center row), and lifetimes (bottom row) for C, AlN, Si, and Li. The figure shows twisted SJ (empty square) and SJB (full square) wave function results with AREPs as well as the ECP pseudopotential (red circle) and all-electron SJ results (red triangle) as a function of the inverse of the number of electrons in the simulation. The ECP pseudopotential and all-electron results are compared against AREP results with the same cell sizes. Monte Carlo error bars are shown for each result. We present the lifetime estimates against experiment (black solid line) for C [51], AlN [52], Si [53], and Li [54]. We also computed DFT lifetime estimates with different positron correlation functionals (dash-dotted lines): D-LDA (violet), BN-LDA (green), B95-GGA (cyan), B15-GGA (red), and KUR-GGA (blue).

meV. The backflow increases the $g(0)$ values. Only in Si we see convergence in PCF with respect to cell size, but changes in $g(0)$ and lifetimes between different cell sizes of the same material are small.

In the largest cells with SJB wave functions, QMC with AREPs overestimates the experimental lifetimes by 2 and 10 ps in C and Si and underestimates them by 2 and 4 ps in AlN and Li. The larger cells with SJ wave functions decreased the lifetimes in C, AlN, and Si by 1 ps and increased by 4 ps in Li. In Si, SJ ECP and core-corrected AREP results agree within error bars. The all-electron lifetime of Li provides a 10 ps increase to the core-corrected AREP result.

We studied the impact of atomic vibrations to lifetime values in Si. We used DFT to calculate the dynamical matrix in a cubic 64-atom simulation cell and diagonalized it to obtain the eigenfrequencies and modes of the atomic vibrations. At temperatures of 0 and 300 K, we sampled a set of occupied states out of the Boltzmann distribution. Displacements were sampled with the Neumann algorithm based on the occupied states. By repeatedly occupying vibrational states and sampling atomic displacements, we produced a set of 100 atomic configurations distributed according to the occupied phonon modes. The average DFT lifetimes increased 2(1) ps compared to the lifetime of the static structure (see Supplemental Material [35]).

The SJB results with AREPs and the reference experimental values are gathered in Table I. See the Supplemental Material [35] for QMC results with core corrections by different DFT functionals.

The SJB lifetime values in C and AlN match almost perfectly with experimental values. Li matches also very well, but the all-electron SJB result could be overestimating

TABLE I. The largest-cell SJB lifetime results obtained with AREPs with ($1/\Gamma$) and without ($1/\Gamma_{\mathrm{QMC}}$) core corrections against experimental lifetimes.

Lifetime (ps)	$1/\Gamma_{\mathrm{QMC}}$	$1/\Gamma$	Experimental Ref.
C	101.7(2)	100.1(2)	98 [51]
AlN	165.1(3)	154.8(3)	157 [52]
Si	237(1)	228(1)	218 [53]
Li	320(1)	287(1)	291 [54]

the experimental value by 7–10 ps, based on the SJ results, although it has to be noted that measurements on Li in the literature are scarce. The overestimation in Si (and Li) might result from the omission of relativistic and bound-state effects in Eq. (2) (both beyond the scope of the present Letter), finite-size effects, fixed-node errors, core electron approximations, or vibrational effects. Finite-size effects have been studied above. Because the backflow decreases the lifetime estimate, the QMC results are not converged with respect to the variational freedom in the wave function, and further improvements might be obtained by, e.g., multideterminant wave functions. The ECP and all-electron calculations with SJB wave functions cannot be computed with current computing resources.

On average, QMC shows better match with experimental lifetimes than DFT for this set of test materials. The mean-square error of QMC predictions against experimental values is $31.3(8)$ ps^2, as opposed to the best performing DFT functional B95-GGA with corresponding value of 89.4 ps^2 (see Supplemental Material [35]). The QMC method is parameter-free, whereas all of the GGA functionals apart from B15-GGA involve one semiempiric parameter, determined by fitting to experimental data [16,17]. The LDA construction is unique and parameter-free, but does not work for the positron lifetime.

In conclusion, we have successfully simulated electron-positron wave functions and computed the positron lifetimes in crystalline C, Si, Li, and AlN with QMC. We studied finite-size effects and different pseudopotentials and included an all-electron calculation. The possibility of vibrational effects greatly affecting lifetimes of thermalized positrons in Si was ruled out.

The results prove that positron lifetime spectroscopy can benefit from the support of parameter-free many-body methods such as QMC calculations. The largest simulation cells in this study are applicable to vacancy calculations, and thus the presented method can be applied to support all fields of modern positron annihilation spectroscopy.

We acknowledge the generous computational resources provided by CSC (Finnish IT Centre for Science) and the use of DECI resource Archer based in Edinburgh, UK, with support from the PRACE aisbl. This work was partially supported by the Academy of Finland Grants No. 285809, No. 293932, No. 319178, No. 334706, and No. 334707.

*Corresponding author.
kristoffer.simula@helsinki.fi

[1] R. A. Ferrell, Theory of positron annihilation in solids, Rev. Mod. Phys. **28**, 308 (1956).
[2] J. Hofierka, B. Cunningham, C. Rawlins, C. Patterson, and D. Green, Many-body theory of positron binding in polyatomic molecules, Nature **606**, 688 (2022).
[3] E. Boroński and R. M. Nieminen, Electron-positron density-functional theory, Phys. Rev. B **34**, 3820 (1986).
[4] N. D. Drummond, P. López Ríos, R. J. Needs, and C. J. Pickard, Quantum Monte Carlo Study of a Positron in an Electron Gas, Phys. Rev. Lett. **107**, 207402 (2011).
[5] F. Tuomisto and I. Makkonen, Defect identification in semiconductors with positron annihilation: Experiment and theory, Rev. Mod. Phys. **85**, 1583 (2013).
[6] R. Krause-Rehberg and H. S. Leipner, *Positron Annihilation in Semiconductors: Defect Studies* (Springer Science & Business Media, New York, 1999), Vol. 127.
[7] R. A. Pethrick, Positron annihilation-a probe for nano-scale voids and free volume?, Prog. Polym. Sci. **22**, 1 (1997).
[8] Y. C. Jean, P. E. Mallon, and D. M. Schrader, *Principles and Applications of Positron and Positronium Chemistry* (World Scientific, Singapore, 2003).
[9] D. Gidley, W. Frieze, T. Dull, J. Sun, A. Yee, C. Nguyen, and D. Yoon, Determination of pore-size distribution in low-dielectric thin films, Appl. Phys. Lett. **76**, 1282 (2000).
[10] N. Segercrantz, J. Slotte, F. Tuomisto, K. Mizohata, and J. Räisänen, Instability of the Sb vacancy in GaSb, Phys. Rev. B **95**, 184103 (2017).
[11] J.-M. Mäki, F. Tuomisto, A. Varpula, D. Fisher, R. U. A. Khan, and P. M. Martineau, Time Dependence of Charge Transfer Processes in Diamond Studied with Positrons, Phys. Rev. Lett. **107**, 217403 (2011).
[12] D. Schödlbauer, G. Kögel, P. Sperr, and W. Triftshäuser, Lifetime measurements with a pulsed slow positron beam, Phys. Status Solidi A **102**, 549 (1987).
[13] A. David, G. Kögel, P. Sperr, and W. Triftshäuser, Lifetime Measurements with a Scanning Positron Microscope, Phys. Rev. Lett. **87**, 067402 (2001).
[14] G. Kontrym-Sznajd, Fermiology via the electron momentum distribution, Low Temp. Phys. **35**, 599 (2009).
[15] In the HF theory, the particles are uncorrelated and the contact pair correlation function is $g(0) = 1$. However, in correlated simulations the value increases as demonstrated in Fig. 1.
[16] B. Barbiellini, M. J. Puska, T. Torsti, and R. M. Nieminen, Gradient correction for positron states in solids, Phys. Rev. B **51**, 7341 (1995).
[17] J. Kuriplach and B. Barbiellini, Improved generalized gradient approximation for positron states in solids, Phys. Rev. B **89**, 155111 (2014).
[18] B. Barbiellini and J. Kuriplach, Proposed Parameter-Free Model for Interpreting the Measured Positron Annihilation Spectra of Materials Using a Generalized Gradient Approximation, Phys. Rev. Lett. **114**, 147401 (2015).
[19] R. Q. Hood, P. R. C. Kent, R. J. Needs, and P. R. Briddon, Quantum Monte Carlo Study of the Optical and Diffusive Properties of the Vacancy Defect in Diamond, Phys. Rev. Lett. **91**, 076403 (2003).
[20] Y. Kita, R. Maezono, M. Tachikawa, M. Towler, and R. J. Needs, *Ab initio* quantum Monte Carlo study of the positronic hydrogen cyanide molecule, J. Chem. Phys. **131**, 134310 (2009).
[21] Y. Kita, M. Tachikawa, N. D. Drummond, and R. J. Needs, A variational Monte Carlo study of positronic compounds using inhomogeneous backflow transformations, Chem. Lett. **39**, 1136 (2010).

[22] D. M. Ceperley and B. J. Alder, Ground State of the Electron Gas by a Stochastic Method, Phys. Rev. Lett. **45**, 566 (1980).

[23] W. M. C. Foulkes, L. Mitas, R. J. Needs, and G. Rajagopal, Quantum Monte Carlo simulations of solids, Rev. Mod. Phys. **73**, 33 (2001).

[24] R. J. Needs, M. D. Towler, N. D. Drummond, and P. López Ríos, Continuum variational and diffusion quantum Monte Carlo calculations, J. Phys.: Condens. Matter **22**, 023201 (2010).

[25] R. J. Needs, M. D. Towler, N. D. Drummond, P. López Ríos, and J. R. Trail, Variational and diffusion quantum Monte Carlo calculations with the CASINO code, J. Chem. Phys. **152**, 154106 (2020).

[26] J. B. Anderson, A random-walk simulation of the Schrödinger equation: H_3^+, J. Chem. Phys. **63**, 1499 (1975).

[27] R. Jastrow, Many-body problem with strong forces, Phys. Rev. **98**, 1479 (1955).

[28] P. López Ríos, A. Ma, N. D. Drummond, M. D. Towler, and R. J. Needs, Inhomogeneous backflow transformations in quantum Monte Carlo calculations, Phys. Rev. E **74**, 066701 (2006).

[29] W. Kohn and L. J. Sham, Self-consistent equations including exchange and correlation effects, Phys. Rev. **140**, A1133 (1965).

[30] P. Giannozzi, S. Baroni, N. Bonini, M. Calandra, R. Car, C. Cavazzoni, D. Ceresoli, G. L. Chiarotti, M. Cococcioni, I. Dabo *et al.*, Quantum ESPRESSO: A modular and open-source software project for quantum simulations of materials, J. Phys. Condens. Matter **21**, 395502 (2009).

[31] T. Torsti, T. Eirola, J. Enkovaara, T. Hakala, P. Havu, V. Havu, T. Höynälänmaa, J. Ignatius, M. Lyly, I. Makkonen *et al.*, Three real-space discretization techniques in electronic structure calculations, Phys. Status Solidi (b) **243**, 1016 (2006).

[32] I. Makkonen, M. Hakala, and M. J. Puska, Modeling the momentum distributions of annihilating electron-positron pairs in solids, Phys. Rev. B **73**, 035103 (2006).

[33] J. P. Perdew, K. Burke, and M. Ernzerhof, Generalized Gradient Approximation Made Simple, Phys. Rev. Lett. **77**, 3865 (1996).

[34] D. Alfè and M. J. Gillan, Efficient localized basis set for quantum Monte Carlo calculations on condensed matter, Phys. Rev. B **70**, 161101(R) (2004).

[35] See Supplemental Material at http://link.aps.org/supplemental/10.1103/PhysRevLett.129.166403 for more discussion on preparation of trial wave functions, wave function optimizations, core corrections in positron lifetimes, total energies, twist averaging, vibrational effects on positron lifetimes, and fitting procedures to pair correlation function QMC data, which includes Refs. [36,37].

[36] D. W. Marquardt, An algorithm for least-squares estimation of nonlinear parameters, J. Soc. Ind. Appl. Math. **11**, 431 (1963).

[37] K. Levenberg, A method for the solution of certain non-linear problems in least squares, Quart. Appl. Math. **2**, 164 (1944).

[38] N. D. Drummond, M. D. Towler, and R. J. Needs, Jastrow correlation factor for atoms, molecules, and solids, Phys. Rev. B **70**, 235119 (2004).

[39] N. D. Drummond and R. J. Needs, Variance-minimization scheme for optimizing Jastrow factors, Phys. Rev. B **72**, 085124 (2005).

[40] C. J. Umrigar, J. Toulouse, C. Filippi, S. Sorella, and R. G. Hennig, Alleviation of the Fermion-Sign Problem by Optimization of Many-Body Wave Functions, Phys. Rev. Lett. **98**, 110201 (2007).

[41] M. Holzmann, R. C. Clay III, M. A. Morales, N. M. Tubman, D. M. Ceperley, and C. Pierleoni, Theory of finite size effects for electronic quantum Monte Carlo calculations of liquids and solids, Phys. Rev. B **94**, 035126 (2016).

[42] C. Lin, F. H. Zong, and D. M. Ceperley, Twist-averaged boundary conditions in continuum quantum Monte Carlo algorithms, Phys. Rev. E **64**, 016702 (2001).

[43] J. R. Trail and R. J. Needs, Smooth relativistic Hartree-Fock pseudopotentials for H to Ba and Lu to Hg, J. Chem. Phys. **122**, 174109 (2005).

[44] J. R. Trail and R. J. Needs, Norm-conserving Hartree-Fock pseudopotentials and their asymptotic behavior, J. Chem. Phys. **122**, 014112 (2005).

[45] M. C. Bennett, G. Wang, A. Annaberdiyev, C. A. Melton, L. Shulenburger, and L. Mitas, A new generation of effective core potentials from correlated calculations: 2nd row elements, J. Chem. Phys. **149**, 104108 (2018).

[46] A. Ma, M. D. Towler, N. D. Drummond, and R. J. Needs, Scheme for adding electron–nucleus cusps to gaussian orbitals, J. Chem. Phys. **122**, 224322 (2005).

[47] G. F. Gribakin, J. A. Young, and C. M. Surko, Positron-molecule interactions: Resonant attachment, annihilation, and bound states, Rev. Mod. Phys. **82**, 2557 (2010).

[48] N. D. Drummond, P. López Ríos, C. J. Pickard, and R. J. Needs, First-principles method for impurities in quantum fluids: Positron in an electron gas, Phys. Rev. B **82**, 035107 (2010).

[49] D. M. Ceperley and M. H. Kalos, *Monte* Carlo Methods in Statistical Physics (Springer, Berlin, 1979).

[50] J. C. Kimball, Short-range correlations and electron-gas response functions, Phys. Rev. A **7**, 1648 (1973).

[51] A. Pu, T. Bretagnon, D. Kerr, and S. Dannefaer, Positron annihilation investigation of vacancies in as-grown and electron-irradiated diamonds, Diam. Relat. Mater. **9**, 1450 (2000).

[52] F. Tuomisto, J.-M. Mäki, T. Y. Chemekova, Y. N. Makarov, O. V. Avdeev, E. N. Mokhov, A. S. Segal, M. G. Ramm, S. Davis, G. Huminic *et al.*, Characterization of bulk AlN crystals with positron annihilation spectroscopy, J. Cryst. Growth **310**, 3998 (2008).

[53] J. Mäkinen, P. Hautojärvi, and C. Corbel, Positron annihilation and the charge states of the phosphorus-vacancy pair in silicon, J. Phys. Condens. Matter **4**, 5137 (1992).

[54] H. Weisberg and S. Berko, Positron lifetimes in metals, Phys. Rev. **154**, 249 (1967).